

## Article

# Methyl Orange Photo-Degradation by TiO<sub>2</sub> in a Pilot Unit under Different Chemical, Physical, and Hydraulic Conditions

Andrea Petrella <sup>1,\*</sup>, Danilo Spasiano <sup>1</sup>, Pinalysa Cosma <sup>2</sup>, Vito Rizzi <sup>2</sup>, Marco Race <sup>3</sup>,  
Maria Cristina Mascolo <sup>3</sup> and Ezio Ranieri <sup>4</sup>

<sup>1</sup> Dipartimento di Ingegneria Civile, Ambientale, Edile, Del Territorio e di Chimica, Politecnico di Bari, Via E. Orabona 4, 70125 Bari, Italy; danilo.spasiano@poliba.it

<sup>2</sup> Dipartimento di Chimica, Università degli Studi di Bari "Aldo Moro", Via E. Orabona 4, 70125 Bari, Italy; pinalysa.cosma@uniba.it (P.C.); vito.rizzi@uniba.it (V.R.)

<sup>3</sup> Dipartimento di Ingegneria Civile e Meccanica, Università degli Studi di Cassino e del Lazio Meridionale, Via di Biasio 43, 03043 Cassino, Italy; marco.race@unicas.it (M.R.); mc.mascolo@unicas.it (M.C.M.)

<sup>4</sup> Dipartimento di Biologia, Università degli Studi di Bari "Aldo Moro", Via E. Orabona 4, 70125 Bari, Italy; ezio.ranieri@uniba.it

\* Correspondence: andrea.petrella@poliba.it; Tel.: +39-(0)8-0596-3275; Fax: +39-(0)8-0596-3635

**Abstract:** The photo-catalytic degradation of a textile azo-dye as Methyl Orange was studied in an innovative unit constituted by a channel over which a layer of titanium dioxide (TiO<sub>2</sub>) catalyst in anatase form was deposited and activated by UVB irradiation. The degradation kinetics were followed after variation of the chemical, physical, and hydraulic/hydrodynamic parameters of the system. For this purpose, the influence of the TiO<sub>2</sub> dosage (g/cm<sup>3</sup>), dye concentration (mg/L), pH of the solution, flow-rate (L/s), hydraulic load (cm), and irradiation power (W) were evaluated on the degradation rates. It was observed that the maximum dosage of TiO<sub>2</sub> was 0.79 g/cm<sup>3</sup> while for higher dosage a reduction of homogeneity of the cement conglomerate occurred. The Langmuir-Hinshelwood (LH) kinetic model was followed up to a dye concentration around 1 mg/L. It was observed that with the increase of the flow rate, an increase of the degradation kinetics was obtained, while the further increase of the flow-rate associated with the modification of the hydraulic load determined a decrease of the kinetic rates. The results also evidenced an increase of the kinetic rates with the increase of the UVB intensity. A final comparison with other dyes such as Methyl Red and Methylene Blue was carried out in consideration of the pH of the solution, which sensibly affected the removal efficiencies.

**Keywords:** photo-catalysis; TiO<sub>2</sub>; azo dye; kinetic study; hydraulic and hydrodynamic parameters



**Citation:** Petrella, A.; Spasiano, D.; Cosma, P.; Rizzi, V.; Race, M.; Mascolo, M.C.; Ranieri, E. Methyl Orange Photo-Degradation by TiO<sub>2</sub> in a Pilot Unit under Different Chemical, Physical, and Hydraulic Conditions. *Processes* **2021**, *9*, 205. <https://doi.org/10.3390/pr9020205>

Academic Editor: María V. López-Ramón

Received: 5 January 2021

Accepted: 19 January 2021

Published: 21 January 2021

**Publisher's Note:** MDPI stays neutral with regard to jurisdictional claims in published maps and institutional affiliations.



**Copyright:** © 2021 by the authors. Licensee MDPI, Basel, Switzerland. This article is an open access article distributed under the terms and conditions of the Creative Commons Attribution (CC BY) license (<https://creativecommons.org/licenses/by/4.0/>).

## 1. Introduction

Emerging contaminants in water and wastewater are chemical compounds produced by industrial practices and anthropogenic activities [1–6] that must be removed due to their potential toxicological effects on human health and the environment [7–13].

For this purpose, Advanced Oxidation Processes (AOPs) are efficient methods to remove from water and wastewater contaminants of organic nature that are not degradable by biological processes [14–16]. Specifically, these treatments result effective for the removal of micro-pollutants as pesticides, personal care products, pharmaceuticals, flame retardants, antifoulants, stabilizers, and plasticizers, which have harmful effects on the reproductive system [8,17–20].

AOPs are processes involving the production of very reactive radical species able to degrade a wide range of biopersistent organic substrates [21–23]. Among these, photo-catalysis is an efficient treatment carried out with a catalyst that generates radicals when irradiated with light of a suitable wavelength [24–28]. TiO<sub>2</sub> has been extensively studied as a catalyst due to its wide band gap (3.2 eV), strong oxidizing power, high resistance to chemicals, nontoxic nature, and low cost [24,29].

The TiO<sub>2</sub> photocatalysis can be applied in the removal of xenobiotic azo dyes from the textile industry such as Methylene Blue, Methyl Red, and Methyl Orange, which tend to bioaccumulate in the environment and have allergenic, carcinogenic, mutagenic, and teratogenic properties. Methylene Blue is used in dye manufacturing industries, plastics, cosmetics, and printing [30,31]. It is a toxic compound since it can cause eye burns, vomiting, jaundice, and diarrhea [32,33]. Methyl Red is used in textile dyeing and paper printing and it is hazardous in case of skin contact (irritant), inhalation, and ingestion [34,35]. Methyl Orange is widely used in dyeing, printing textiles, and paper industries. Methyl Orange is the common name of a water-soluble aromatic synthetic compound (C<sub>14</sub>H<sub>14</sub>N<sub>3</sub>NaO<sub>3</sub>S) containing an azo group (–N=N–). This molecule is a toxic compound and can cause hypersensitivity, allergies and may be fatal if inhaled [31,36]. The main environmental damage caused by the textile industry is the release of untreated effluents into the water bodies, corresponding to ~80% of the total emissions [37].

The aim of this paper was to study the UVB photo-catalytic degradation of Methyl Orange in water and wastewater by the use of an innovative unit [38–40]. The photocatalytic system was a recirculating plant formed of two tanks connected by a channel over which anatase TiO<sub>2</sub> was deposited and UVB irradiated. The influence of the TiO<sub>2</sub> dosage (g/cm<sup>3</sup>), dye concentration  $c_0$  (mg/L), pH of the solution, flow-rate  $Q$  (L/s), hydraulic load  $h_w$  (cm), and irradiation power (W) were evaluated on the degradation kinetics of this hazardous dye. Moreover, the removal efficiencies of Methyl Orange were compared with those of other textile dyes such as Methyl Red and Methylene Blue in order to have more detailed information about the treatment of these harmful compounds through this unit.

## 2. Experimental Section

Anatase titanium dioxide (TiO<sub>2</sub>) was provided by Adriatica Legnami s.r.l., Italy, and was characterized by 0.15 μm average grain size and 3.85 g/cm<sup>3</sup> specific gravity. Methyl Orange (MO), pure chemical from Sigma Aldrich, was used to prepare the synthetic solutions in tap water (pH = 7.5) and distilled water (pH = 6). Moreover, Methyl Red (MR) and Methylene Blue (MB), pure chemicals from Sigma Aldrich, were also used to prepare tap and distilled water solutions in order to make a comparison.

The determination of the residual dye concentrations was obtained by a UV-Vis spectrophotometer Mod. UVIKON 942 from Kontron Instruments, Augsburg, Germany.

The unit which was used for the experimental tests is depicted in Figure 1. Specifically, Figure 1A,B report the overview and the top view schemes of the system, respectively. Figure 1C represents the real overview of the laboratory scale pilot plant. It was characterized by a channel (c) (15 cm width, 185 cm length) over which layers of cement mortars (0.5 mm thickness) with different TiO<sub>2</sub> concentrations (0.16 g/cm<sup>3</sup>, 0.39 g/cm<sup>3</sup>, 0.55 g/cm<sup>3</sup>, 0.79 g/cm<sup>3</sup>) were deposited. The dye influent solution was kept under UVB irradiation in contact with the catalyst. For this purpose, three low-pressure UVB lamps (40 W each, λ<sub>em</sub> = 312 nm), Vilber-Lourmat (Collégien, France), were used. The system was characterized by an upper reservoir with manifolds (a) which allowed for the change of the treated volume solution associated with the modification of the hydraulic load ( $h_w$ ) with consequent variation of the flow-rates ( $Q$ ). The introduction of layers of different thicknesses (1.5, 1.0 and 0.5 mm; 11 × 70 cm) into an opening of this tank allowed for the modification of the flow-rate ( $Q$ ), keeping constant the hydraulic load ( $h_w$ ). The system was also characterized by a bottom reservoir (b) with similar capacity to the former and equipped with a piezometric tube. A pump (d) (Mod. CPM 130, Pedrollo, Milan, Italy; 0.37 kW, 230 V, 50 Hz) was used for the recirculation of the influent solution through the unit. Table 1 represents a summary of the tests carried out in the present investigation.

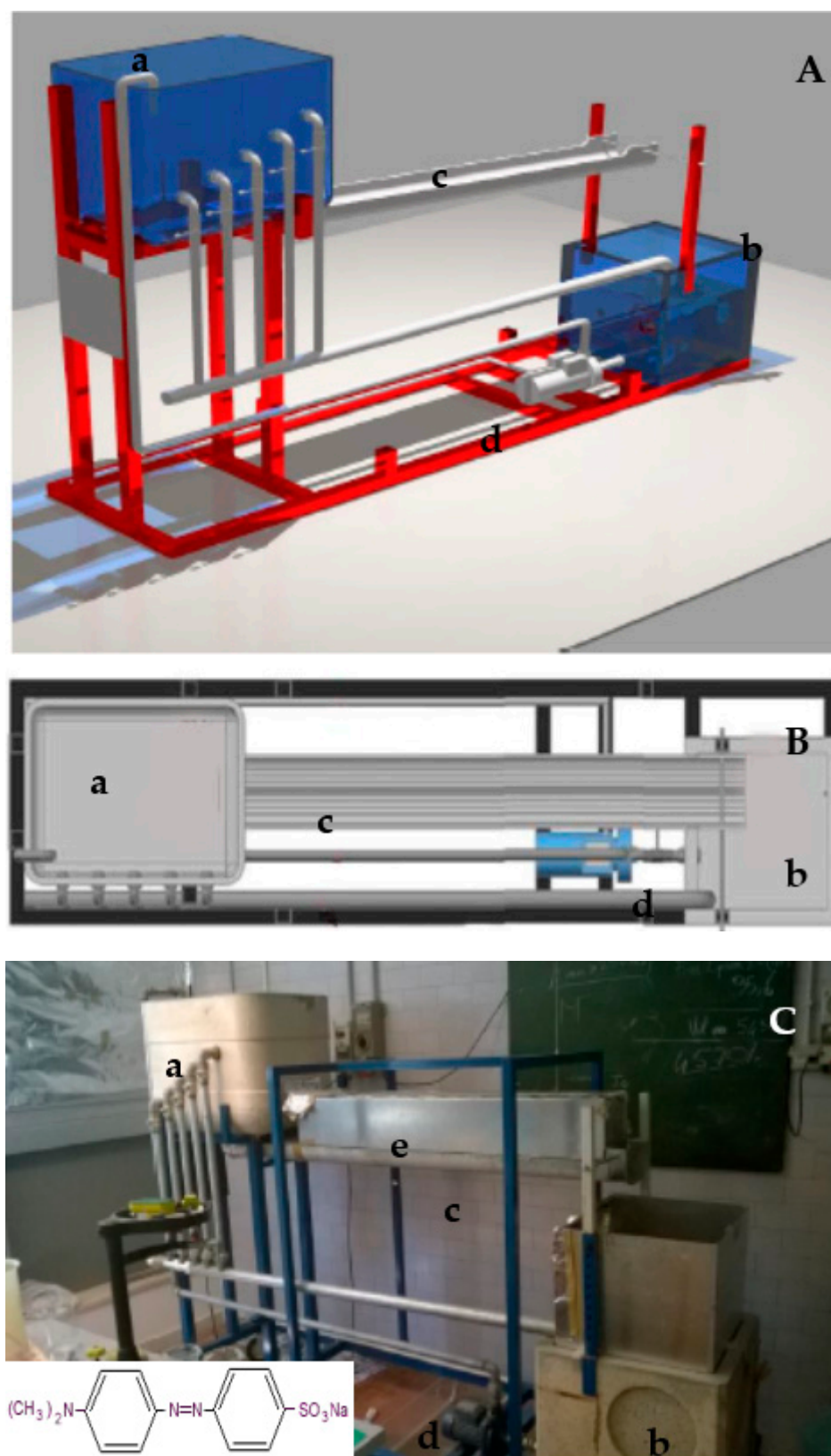


**Figure 1.** (A) Overview scheme and (B) top view scheme of the laboratory scale pilot plant. (C) Picture of the unit. (a) Upper reservoir, (b) bottom reservoir, (c) channel, (d) pump, (e) UVB lamp.

**Table 1.** Summary of the tests carried out in the present investigation.  $c_0$  = initial dye concentration,  $V_{sol}$  = volume of the influent solution,  $Q$  = flow-rate,  $h_w$  = hydraulic load,  $l_w$  = irradiated liquid width in the channel,  $l_c$  = irradiated liquid length in the channel,  $l_d$  = irradiated liquid depth in the channel,  $V_{irr}$  = irradiated volume ( $l_w \times l_c \times l_d$ ) of the liquid in the channel,  $I_{rt}$  = irradiated retention time ( $V_{irr}/Q$ ), irradiation power (W), pH.

Test No.	$c_0$ (mg/L)	$TiO_2$ (g/cm <sup>3</sup> )	$V_{sol}$ (L)	$Q$ (L/s)	$h_w$ (cm)	$l_w$ (cm)	$l_c$ (cm)	$l_d$ (cm)	$V_{irr}$ (L)	$I_{rt}$ (s)	Light	Power (W)	pH
1	0.7	0.16	60	0.066	13.5	14	140	0.65	1.27	17.9	yes	120	7.5
2	0.7	0.39	60	0.066	13.5	14	140	0.65	1.27	17.9	yes	120	7.5
3	0.7	0.55	60	0.066	13.5	14	140	0.65	1.27	17.9	yes	120	7.5
4	0.7	0.79	60	0.066	13.5	14	140	0.65	1.27	17.9	yes	120	7.5
5	0.7	0.85	60	0.066	13.5	14	140	0.65	1.27	17.9	yes	120	7.5
6	0.7	0.95	60	0.066	13.5	14	140	0.65	1.27	17.9	yes	120	7.5
7	0.3, 0.7, 1.2, 2.5, 5	0.79	60	0.066	13.5	14	140	0.65	1.27	17.9	yes	120	7.5
8	0.3, 0.7, 1.2, 2.5, 5	0.79	60	0.147	13.5	15	140	0.79	1.66	10.5	yes	120	7.5
9	0.3, 0.7, 1.2, 2.5, 5	0.79	60	0.210	13.5	15	140	0.85	1.78	7.9	yes	120	7.5
10	0.3, 0.7, 1.2, 2.5, 5	0.79	60	0.305	13.5	15	140	1.05	2.20	6.7	yes	120	7.5
11	0.7	0.79	72.5	0.355	18	15	140	1.08	2.30	5.8	yes	120	7.5
12	0.7	0.79	90	0.408	22.5	15	140	1.12	2.35	5.2	yes	120	7.5
13	0.7	0.79	105	0.441	27	15	140	1.16	2.45	4.9	yes	120	7.5
14	0.7	0	60	0.305	13.5	15	140	1.05	2.20	6.7	yes	120	7.5
15	0.7	0.79	60	0.305	13.5	15	140	1.05	2.20	6.7	no	no	7.5
16	0.7	0.79	60	0.305	13.5	15	140	1.05	2.20	6.7	yes	40	7.5
17	0.7	0.79	60	0.305	13.5	15	140	1.05	2.20	6.7	yes	80	7.5
18	0.7	0.79	60	0.305	13.5	15	140	1.05	2.20	6.7	yes	120	6.0

### 3. Results and Discussion

The first set of photocatalytic experiments was carried out at different  $TiO_2$  dosage, tests no. 1–6 (Figure 2), constant flow-rate ( $Q = 0.066$  L/h), the hydraulic load ( $h_w = 13.5$  cm), and the influent substrate concentration ( $c_0 = 0.7$  mg/L) as reported in Table 1. The processes described in this paper, at low initial dye concentration, may be approximated by the “pseudo-first-order” equation,

$$\ln(c/c_0) = -k \times \theta \times t \quad (1)$$

i.e., the Langmuir–Hinshelwood (LH) kinetic model. In this equation,  $c_0$  (mg/L) is the starting concentration of the substrate and  $c$  (mg/L) is the concentration of the dye at specific time intervals, while  $k$  is the apparent rate constant ( $\text{min}^{-1}$ ) and  $\theta$  represents the number of the surface active sites present on the catalyst surface [41–43]. The trend reported in the inset of Figure 2 is in agreement with this model, accordingly after linear correlation the apparent rate constant is represented by the slope. Figure 2 shows that the degradation rate increased with the increase of the catalyst concentration due to the growing number of the active sites necessary for the photocatalytic oxidation. Theoretically, an improvement of the results could be obtained with a further increase of oxide concentration but a reduction of homogeneity was observed which was detrimental for the process since leaching of the

catalyst from the cement conglomerate occurred. In this respect, the maximum dosage of  $\text{TiO}_2$  was  $0.79 \text{ g/cm}^3$ .

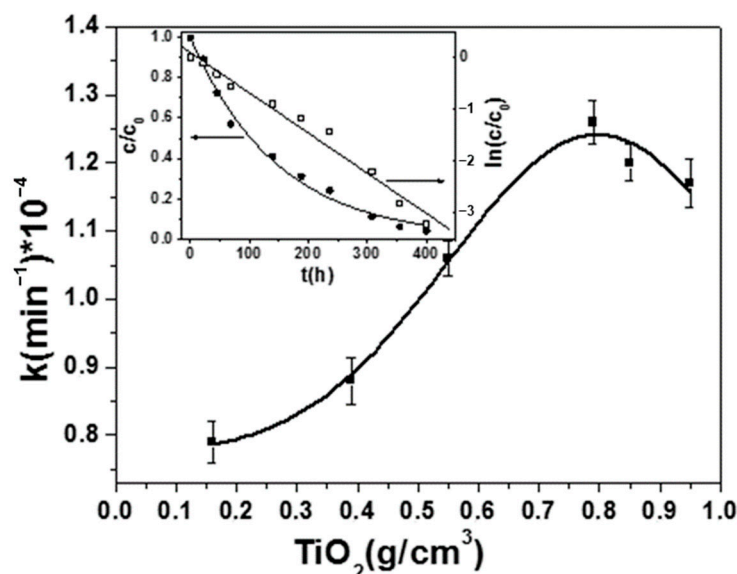


**Figure 2.** Influence of the  $\text{TiO}_2$  dosage on the degradation rate (Methyl Orange (MO) =  $0.7 \text{ mg/L}$ ;  $Q = 0.066 \text{ L/s}$ ,  $h_w = 13.5 \text{ cm}$ , tests no. 1–6). In the inset:  $c/c_0$  vs.  $t$  and  $\ln(c/c_0)$  vs.  $t$  correlations relative to test no. 4 (MO =  $0.7 \text{ mg/L}$ ;  $\text{TiO}_2 = 0.79 \text{ g/cm}^3$ ;  $Q = 0.066 \text{ L/s}$ ,  $h_w = 13.5 \text{ cm}$ ).

The second set of experiments (Table 1, test no. 7) was carried out at different substrate concentration ( $0.3$ – $5.0 \text{ mg/L}$  range, Figure 3), constant flow-rate ( $0.066 \text{ L/h}$ ), the hydraulic load ( $h_w = 13.5 \text{ cm}$ ), and with  $0.79 \text{ g/cm}^3$  catalyst dosage because, as formerly reported, it is the titania concentration corresponding to the highest degradation rate. It can be observed that the best performance was obtained with a substrate concentration corresponding to  $0.7 \text{ mg/L}$  (Figure 3A), while lower values were obtained with the  $[\text{MO}]$  increase. Basically, the Langmuir–Hinshelwood (LH) kinetic model was not followed at higher concentrations due to the absorption of the UV radiation operated by the dye molecules which limited the photocatalytic process thus becoming bare photolysis.

In fact, the photocatalysis of the adsorbed substrate is based on two simultaneous reactions, oxidation from photogenerated holes ( $h^+$ ) and reduction from photogenerated electrons ( $e^-$ ) after excitation of titania with UVB light. Specifically, the oxidation of the adsorbed water by the holes generates hydroxyl radicals  $-\text{OH}$  while the reduction of the oxygen by the electrons generates superoxide radicals  $-\text{O}_2^-$ , both reacting with the organic molecule [44,45].

The increased concentration of the dye solution in the  $1.2$ – $5 \text{ mg/L}$  range decreased the interaction of light with the catalyst surface; accordingly, the combined effect of UV radiation and titania started to be less effective.

Figure 3B shows the temporal evolution of the MO UV–vis absorption spectrum for a  $5 \text{ mg/L}$  influent solution. The spectrum shows a maximum corresponding to the  $\pi \rightarrow \pi^*$  transitions of the dimethylamino electron donors at  $470 \text{ nm}$  and a  $270 \text{ nm}$  peak associated to  $\pi \rightarrow \pi^*$  transitions of the aromatic rings. A UV–vis quenching and blue-shift of the MO absorption peak during the kinetic experiments was observed, which confirmed the degradation of the substrate associated with the removal of the N-methyl groups [46].

The third set of experiments (Table 1, tests no. 7, 8, 9, 10) was carried out at different flow rates ( $0.066 \text{ L/s}$ ,  $0.147 \text{ L/s}$ ,  $0.210 \text{ L/s}$ ,  $0.305 \text{ L/s}$ ) with a substrate concentration in the range of  $0.3$ – $5.0 \text{ mg/L}$ , constant catalyst dosage  $0.79 \text{ g/cm}^3$ . The variation of the flow rate, constant hydraulic load ( $h_w = 13.5 \text{ cm}$ ) was obtained by the introduction of layers of different thicknesses ( $1.5$ ,  $1.0$ , and  $0.5 \text{ mm}$ ;  $11 \times 70 \text{ cm}$ ) into an opening of this tank. It was observed that with the increase of the flow rate, an increase of the degradation kinetics was

obtained. This result can be ascribed to an increasingly higher dissolution of the dissolved oxygen into the water solution, which affected the kinetic rates because of the increase of the photogenerated radicals reacting with the substrate. Moreover, a faster re-circulation of the solution and an increase of the irradiated volume ( $V_{irr}$ , Table 1) can also explain these trends. Furthermore, in this case, it can be observed that the best performance was obtained with a substrate concentration corresponding to 0.7 mg/L, while lower values were obtained with a further increase up to 5 mg/L. Figure 4B shows the kinetic trend and the temporal evolution of the MO UV-vis absorption spectrum for a 0.7 mg/L influent solution characterized by quenching and blue-shift of the maximum absorption peak.

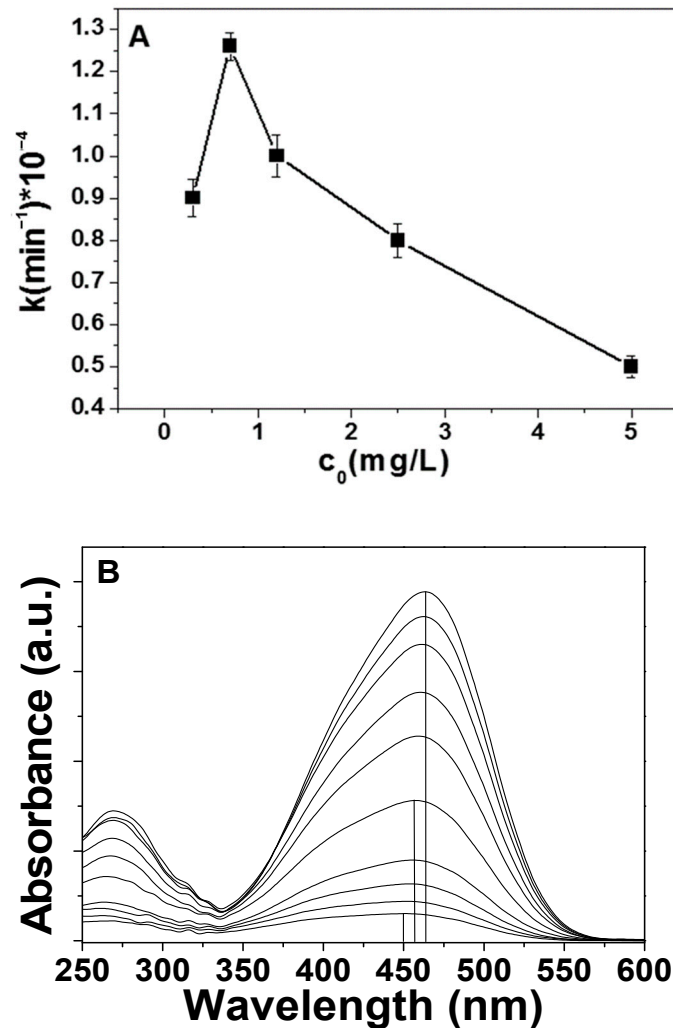
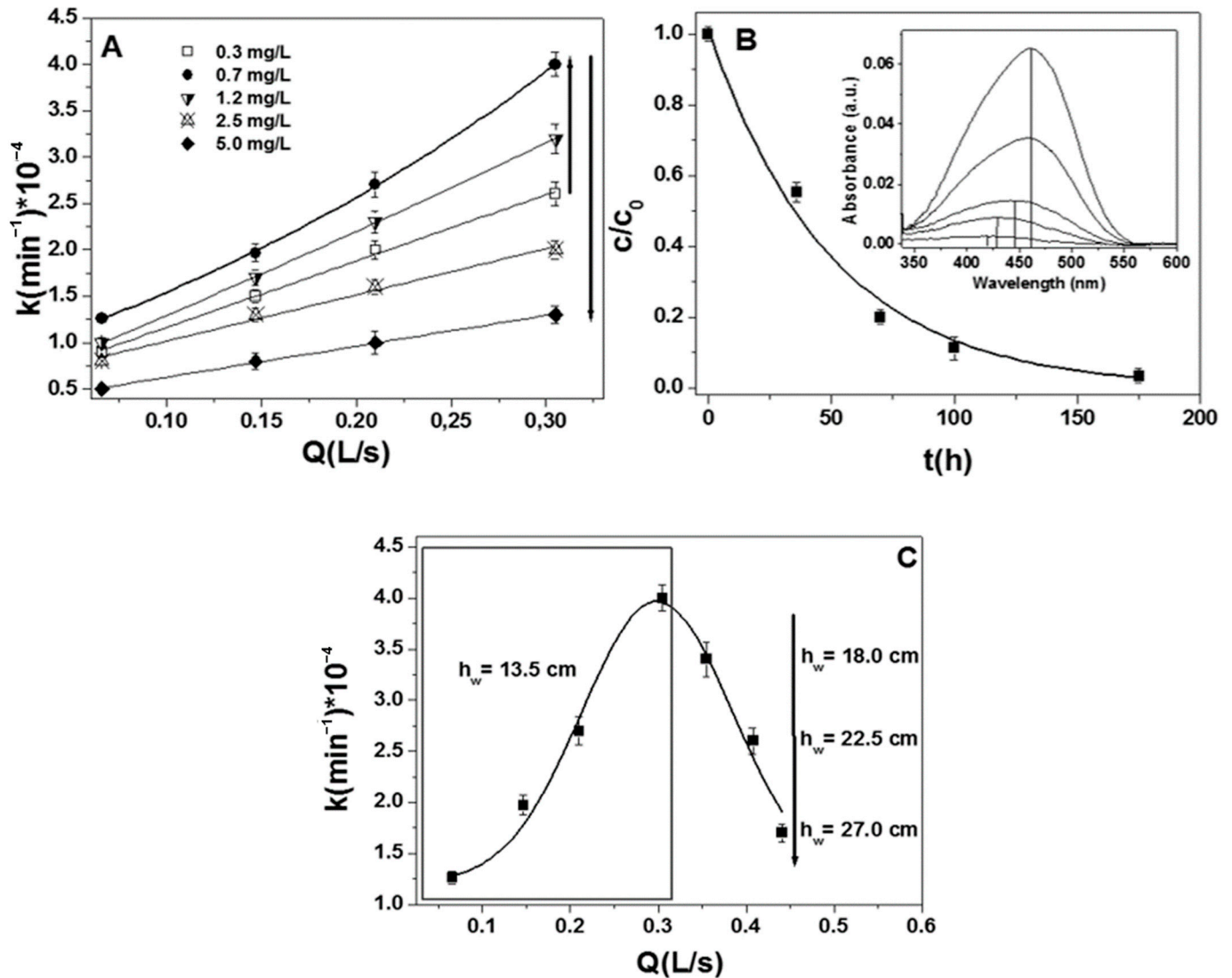


Figure 3. (A) Influence of the dye concentration  $c_0$  on the degradation rate ( $\text{TiO}_2 = 0.79 \text{ g/cm}^3$ ;  $Q = 0.066 \text{ L/s}$ ,  $h_w = 13.5 \text{ cm}$ , test no. 7). (B) MO UV-Vis absorption spectrum decay during the photo-degradation. MO = 5 mg/L;  $\text{TiO}_2 = 0.79 \text{ g/cm}^3$ ;  $Q = 0.066 \text{ L/s}$ ,  $h_w = 13.5 \text{ cm}$ .

The fourth set of experiments (Table 1, tests no. 10, 11, 12, 13) was carried out at different hydraulic loads ( $h_w$ ) corresponding to different solution volumes  $V_{sol}$  (60 L, 72.5 L, 90 L and 105 L) and flow-rates  $Q$  (0.305 L/s, 0.355 L/s, 0.408 L/s, 0.441 L/s), constant substrate concentration ( $c_0 = 0.7 \text{ mg/L}$ ), and the catalyst dosage ( $0.79 \text{ g/cm}^3$ ). These results were combined with the former results regarding the variation of the flow rates at the same hydraulic load (0.066 L/s, 0.147 L/s, 0.210 L/s, 0.305 L/s) and reported in Figure 4C. On the contrary of what expected, the further increase of the flow rates associated with the modification of the hydraulic load determined a decrease of the kinetics because of the increasingly large volume ( $V_{sol}$ ) of the dye solution to treat (60 L for 0.305 L/s, 72.5 L for

0.355 L/s, 90 L for 0.408 L/s, 105 L for 0.441 L/s) and of the ever shorter catalysts/substrate contact times ( $I_{rt}$ ) (6.7 s for 0.305 L/s, 5.8 s for 0.355 L/s, 5.2 s for 0.408 L/s, 5.2 s for 0.441 L/s, Table 1).



**Figure 4.** (A) Influence of the flow rate at different dye concentrations ( $\text{TiO}_2 = 0.79 \text{ g/cm}^3$ ,  $h_w = 13.5 \text{ cm}$ , tests no. 7, 8, 9, 10). (B) kinetic curve relative to the experiment carried out with MO = 0.7 mg/L;  $\text{TiO}_2 = 0.79 \text{ g/cm}^3$ ,  $Q = 0.305 \text{ L/h}$ ,  $h_w = 13.5 \text{ cm}$  and in the inset the relative UV-vis absorption spectrum decay. (C) kinetics obtained at different hydraulic parameters (flow rate  $Q$ , hydraulic load  $h_w$ , MO = 0.7 mg/L;  $\text{TiO}_2 = 0.79 \text{ g/cm}^3$ , tests no. 7–13).

From the kinetic study carried out at variable hydraulic and hydrodynamic conditions, it was observed that the best results were detected at  $Q = 0.305 \text{ L/s}$  and  $h_w = 13.5 \text{ cm}$  hydraulic load (corresponding to the maximum of the curve, Figure 4C) with a dye concentration and  $\text{TiO}_2$  dosage, respectively, ranging 0.7 mg/L and  $0.79 \text{ g/cm}^3$ .

Figure 5 reports how the combined effect of UVB light and catalyst (test no. 10) affects the degradation of the substrate and influences the kinetic rates (fifth set of tests). For this purpose, the photolytic and the bare adsorption tests (tests no. 14 and 15) resulted very slow, thus showing limited effects on the dye removal.

The synergistic combination of irradiation and catalyst can be influenced by the intensity of UVB light. It was studied and represented in Figure 6 reporting the measurements carried out at  $Q = 0.305 \text{ L/s}$ ,  $h_w = 13.5 \text{ cm}$ ,  $c_0 = 0.7 \text{ mg/L}$ , and  $\text{TiO}_2 = 0.79 \text{ g/cm}^3$ . In the present case, the tests were performed with 40 W, 80 W, and 120 W (tests no. 10, 16, and

17) and the results demonstrated the increase of the kinetic rates with the increase of the UVB intensity, although it was observed that passing from 40 W to 120 W the apparent rate constant only doubled.

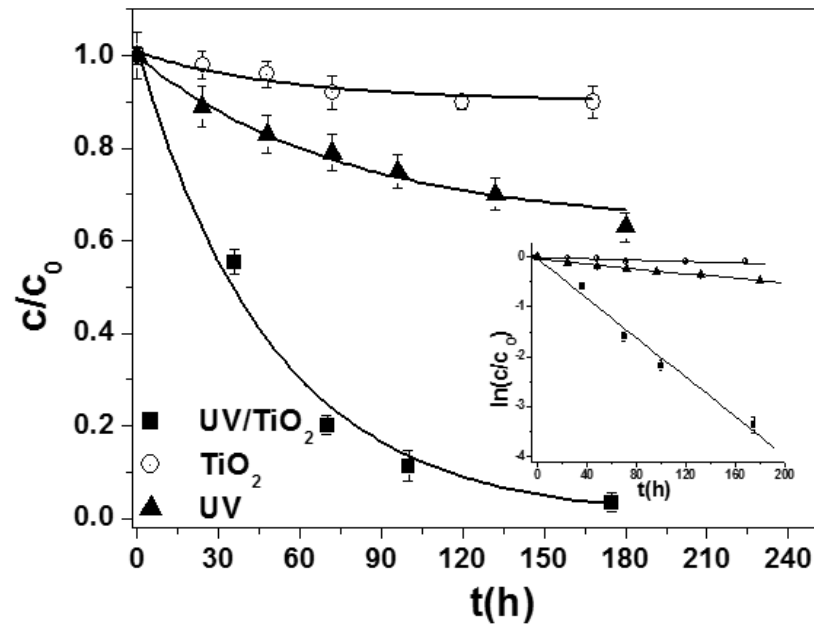


**Figure 5.** Kinetic trends for the UV/TiO<sub>2</sub> photo-catalysis (test no. 10), UVB photolysis (test no. 14), adsorption (only TiO<sub>2</sub>, test no. 15), MO = 0.7 mg/L; TiO<sub>2</sub> = 0.79 g/cm<sup>3</sup>; Q = 0.305 L/s;  $h_w = 13.5$ . In the inset:  $\ln(c/c_0)$  vs.  $t$  correlations.

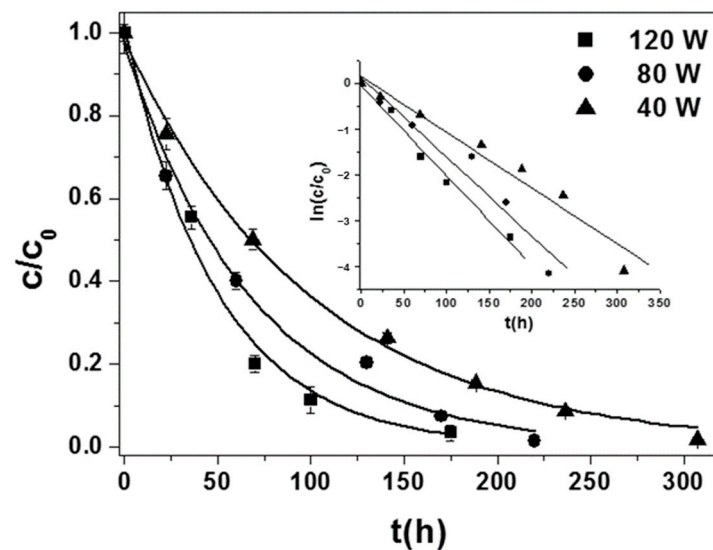


**Figure 6.** Kinetic trends for the UV/TiO<sub>2</sub> photo-catalysis at different UVB intensity (tests no. 10, 16, 17), MO = 0.7 mg/L; TiO<sub>2</sub> = 0.79 g/cm<sup>3</sup>; Q = 0.305 L/s;  $h_w = 13.5$ . In the inset:  $\ln(c/c_0)$  vs.  $t$  correlations.

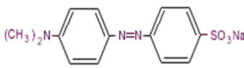
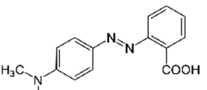
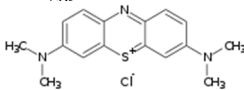
Similar results were also observed in the case of other dye substrates as Methyl Red while in the case of Methylene Blue, the kinetic rates dramatically increased from 40 W to 120 W, all the other chemical and hydraulic/hydrodynamic parameters were constant (Table 2).

Basically, the pH of the solution and the pH at zero point charge of TiO<sub>2</sub> (pH<sub>ZPC</sub>) can influence these results because the surface state of the catalyst and the charge of the substrate functional groups are affected by pH variations [47].

Specifically, the  $\text{TiO}_2$  surface is negative ( $\text{Ti-O}^-$ ) at pH higher than the catalyst  $\text{pH}_{\text{zpc}}$  (6.8), while the  $\text{TiO}_2$  surface is positive ( $\text{Ti-OH}_2^+$ ) at pH lower than the catalyst  $\text{pH}_{\text{zpc}}$  [41,47]. In the present case, the solutions were prepared in tap water with a pH around 7.5.

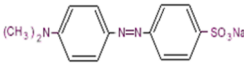
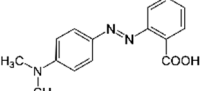
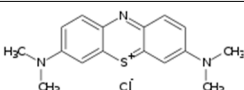
The non-polar Methyl Red is not affected by these operative conditions, while Methylene Blue is a cationic dye at all pH [41,47,48]. Methyl Orange is instead characterized by a negative charge; accordingly, the lowest kinetics of MO can be ascribed to the Coulombic repulsion between the negative sulfonate groups of the dye and the negative charged surface of  $\text{TiO}_2$  [41,47]. Methyl Red is sorbed by secondary Van der Waals bonds between the hydroxyl and amino functional groups of this substrate and the catalyst, while the best performances with Methylene Blue can be explained by the adsorption of the positive charged dye onto the negative charged catalyst surface (Table 2) [48]. The better interaction between the MB functionalities and the  $\text{TiO}_2$  surface can also explain the large increase of the kinetic rate with the increase of the UVB intensity as regard to the other dyes.

**Table 2.** (A) Apparent rate constants for the UV/ $\text{TiO}_2$  photo-catalysis at different UVB intensity (tests no. 10, 16, 17) for Methyl Orange, Methyl Red, and Methylene Blue, [dye] = 0.7 mg/L;  $\text{TiO}_2$  = 0.79 g/cm<sup>3</sup>; tap water (pH = 7.5);  $Q$  = 0.305 L/s;  $hw$  = 13.5.

Dye	Molecular Structure	Power (W)	$k$ (min <sup>-1</sup> ) × 10 <sup>-4</sup>
Methyl Orange		40	2 ± 0.2
		80	2.9 ± 0.3
		120	4 ± 0.1
Methyl Red		40	2.6 ± 0.1
		80	3.7 ± 0.1
		120	5.7 ± 0.3
Methylene Blue		40	8.8 ± 0.4
		80	19 ± 0.5
		120	35 ± 0.5

It can be also observed that if the measurements were carried out in distilled water (pH = 6), with all the other chemical, physical, and hydraulic/hydrodynamic parameters constant, the kinetics resulted different (tests no. 18). Under these conditions, the interactions of the Methyl Orange functional groups with the catalyst surface were improved with an increase of the value of the apparent rate constant in the range of 40%, quite similar to that obtained with Methyl Red which, as reported before, is not affected by the pH. The kinetic rate of the Methylene Blue showed a decrease in the range of the 20% associated with a decrease of the interactions between the positive charged dye and the more positive catalyst surface (Table 3, Figure 7).

**Table 3.** (A) Apparent rate constants for the UV/ $\text{TiO}_2$  photo-catalysis at 120 W (tests no. 18) for Methyl Orange, Methyl Red, and Methylene Blue, [dye] = 0.7 mg/L;  $\text{TiO}_2$  = 0.79 g/cm<sup>3</sup>; distilled water (pH = 6);  $Q$  = 0.305 L/s;  $hw$  = 13.5.

Dye	Molecular Structure	Power (W)	$k$ (min <sup>-1</sup> ) × 10 <sup>-4</sup>
Methyl Orange		120	5.6 ± 0.3
Methyl Red		120	5.2 ± 0.3
Methylene Blue		120	29 ± 0.5

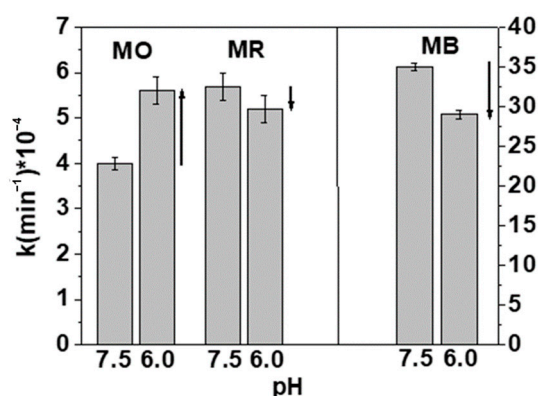


**Figure 7.** Apparent rate constants in tap water (pH = 7.5) and distilled water (pH = 6) at 120 W (tests no. 10 and 18) for Methyl Orange (MO), Methyl Red (MR), and Methylene Blue (MB), [dye] = 0.7 mg/L;  $\text{TiO}_2$  = 0.79 g/cm<sup>3</sup>;  $Q$  = 0.305 L/s;  $hw$  = 13.5.

#### 4. Conclusions

A laboratory-scale unit was employed to study the UVB photo-catalytic degradation of Methyl Orange by anatase  $\text{TiO}_2$  embedded in a cement matrix and deposited onto a channel of a recirculating system. The influence of the  $\text{TiO}_2$  dosage (g/cm<sup>3</sup>), dye concentration (mg/L), flow-rate (L/s), hydraulic load (cm) and irradiation power (W), and pH of the solution were evaluated on the degradation rates.

The degradation rate increased with the increase of the catalyst concentration due to the growing number of the active sites necessary for the photocatalytic oxidation. The maximum dosage of  $\text{TiO}_2$  was 0.79 g/cm<sup>3</sup> and with a further increase of oxide concentration, a reduction of homogeneity was observed, which was detrimental for the process since leaching of the catalyst from the cement conglomerate occurred.

The best performance was obtained with a substrate concentration corresponding to 0.7 mg/L, while lower values were obtained with a further increase up to 5 mg/L. The Langmuir–Hinshelwood (LH) kinetic model was followed up to ~1 mg/L concentration; at higher concentrations, a bare photolysis process occurred.

It was observed that with the increase of the flow rate an increase of the degradation kinetics was obtained due to the increasingly higher dissolution of the oxygen into the water solution, the faster re-circulation of the solution, and the increase of the irradiated volume.

The further increase of the flow rates associated with the modification of the hydraulic load determined a decrease of the kinetic rates because of the increasingly large volume of the dye solution to treat and of the ever shorter catalysts/substrate contact times.

The photolytic and the bare adsorption tests showed very slow rates thus demonstrating the effective synergistic action of the UVB light/catalyst system on the dye removal.

An increase of the kinetic rates with the increase of the UVB intensity was observed, although the values only doubled from 40 W to 120 W.

A comparison with other dyes was carried out. Similar results were observed in the case of Methyl Red, while in the case of Methylene Blue, the kinetic rates dramatically increased from 40 W to 120 W.

The pH of the solution influenced these results because the charge of the catalyst surface and the charge of the substrate functional groups were affected by pH variations. For this reason, different results were observed with the different dyes at the pH of tap water and at the pH of distilled water.

As a final remark, the kinetic trends reported in this paper are not easily comparable with literature results due to the different operative conditions of the systems. In particular, in this paper, the measurements were carried out in a re-circulating unit where  $\text{TiO}_2$  was immobilized onto a channel. Moreover, in this case, the  $\text{TiO}_2$ /dye molar ratio was 2 or 3 orders of magnitude lower and the catalyst particle size on the order of micron (lower specific surface area) was deposited and not suspended.

The operations were also carried out with low-pressure UVB lamps and no thermal activation of the film or additions of other oxidants as  $O_2$ ,  $H_2O_2$ ,  $S_2O_8^{2-}$  were carried out to improve sorption/degradation of Methyl Orange.

**Author Contributions:** Conceptualization, D.S.; methodology, M.R.; validation, M.R.; formal analysis, V.R.; investigation, A.P.; resources, A.P.; data curation, M.C.M.; writing—original draft preparation, A.P.; writing—review and editing, P.C.; visualization, E.R.; supervision, D.S. All authors have read and agreed to the published version of the manuscript.

**Funding:** This research received no external funding.

**Data Availability Statement:** Data sharing not applicable.

**Conflicts of Interest:** The authors declare no conflict of interest.

## References

1. Joseph, L.; Jun, B.M.; Jang, M.; Park, C.M.; Muñoz-Senmache, J.C.; Hernández-Maldonado, A.J.; Heyden, A.; Yu, M.; Yoon, Y. Removal of contaminants of emerging concern by metal-organic framework nanoadsorbents: A review. *Chem. Eng. J.* **2019**, *369*, 928–946. [[CrossRef](#)]
2. García-Córcoles, M.T.; Rodríguez-Gómez, R.; de Alarcón-Gómez, B.; Çipa, M.; Martín-Pozo, L.; Kauffmann, J.M.; Zafra-Gómez, A. Chromatographic methods for the determination of emerging contaminants in natural water and wastewater samples: A review. *Crit. Rev. Anal. Chem.* **2019**, *49*, 160–186. [[CrossRef](#)] [[PubMed](#)]
3. Alimi, O.S.; Budariz, J.F.; Hernandez, L.M.; Tufenkji, N. Microplastics and nanoplastics in aquatic environments: Aggregation, deposition, and enhanced contaminant transport. *Environ. Sci. Technol.* **2018**, *52*, 1704–1724. [[CrossRef](#)] [[PubMed](#)]
4. Petrella, A.; Petruzzelli, V.; Basile, T.; Petrella, M.; Boghetich, G.; Petruzzelli, D. Recycled porous glass from municipal/industrial solid wastes sorting operations as a lead ion sorbent from wastewaters. *React. Funct. Polym.* **2010**, *70*, 203–209. [[CrossRef](#)]
5. Petrella, A.; Petrella, M.; Boghetich, G.; Basile, T.; Petruzzelli, V.; Petruzzelli, D. Heavy metals retention on recycled waste glass from solid wastes sorting operations: A comparative study among different metal species. *Ind. Eng. Chem. Res.* **2012**, *51*, 119–125. [[CrossRef](#)]
6. Tammaro, M.; Fiandra, V.; Mascolo, M.C.; Salluzzo, A.; Riccio, C.; Lancia, A. Photocatalytic degradation of atenolol in aqueous suspension of new recyclable catalysts based on titanium dioxide. *J. Environ. Chem. Eng.* **2017**, *5*, 3224–3234. [[CrossRef](#)]
7. Quesada, H.B.; Baptista, A.T.A.; Cusioli, L.F.; Seibert, D.; de Oliveira Bezerra, C.; Bergamasco, R. Surface water pollution by pharmaceuticals and an alternative of removal by low-cost adsorbents: A review. *Chemosphere* **2019**, *222*, 766–780. [[CrossRef](#)]
8. Sillanpää, M.; Ncibi, M.C.; Matilainen, A.; Vepsäläinen, M. Removal of natural organic matter in drinking water treatment by coagulation: A comprehensive review. *Chemosphere* **2018**, *190*, 54–71. [[CrossRef](#)]
9. Petrella, A.; Spasiano, D.; Rizzi, V.; Cosma, P.; Race, M.; De Vietro, N. Thermodynamic and kinetic investigation of heavy metals sorption in packed bed columns by recycled lignocellulosic materials from olive oil production. *Chem. Eng. Comm.* **2019**, 1–16. [[CrossRef](#)]
10. Bai, X.; Acharya, K. Removal of seven endocrine disrupting chemicals (EDCs) from municipal wastewater effluents by a freshwater green alga. *Environ. Pollut.* **2019**, *247*, 534–540. [[CrossRef](#)] [[PubMed](#)]
11. Spasiano, D.; Luongo, V.; Petrella, A.; Alfè, M.; Pirozzi, F.; Fratino, U.; Piccinni, A.F. Preliminary study on the adoption of dark fermentation as pretreatment for a sustainable hydrothermal denaturation of cement-asbestos composites. *J. Clean. Prod.* **2017**, *166*, 172–180. [[CrossRef](#)]
12. Petrella, A.; Petruzzelli, V.; Ranieri, E.; Catalucci, V.; Petruzzelli, D. Sorption of Pb(II), Cd(II) and Ni(II) from single- and multimetal solutions by recycled waste porous glass. *Chem. Eng. Commun.* **2016**, *203*, 940–947. [[CrossRef](#)]
13. Rizzi, V.; D’Agostino, F.; Gubitosa, J.; Fini, P.; Petrella, A.; Agostiano, A.; Semeraro, P.; Cosma, P. An alternative use of olive pomace as a wide-ranging bioremediation strategy to adsorb and recover disperse orange and disperse red industrial dyes from wastewater. *Separations* **2017**, *4*, 29. [[CrossRef](#)]
14. Zazou, H.; Afanga, H.; Akhouairi, S.; Ouchtak, H.; Addi, A.A.; Akbour, R.A.; Assabane, A.; Douch, J.; Elmchaour, A.; Duplay, J.; et al. Treatment of textile industry wastewater by electrocoagulation coupled with electrochemical advanced oxidation process. *J. Water Process Eng.* **2019**, *28*, 214–221. [[CrossRef](#)]
15. Brillas, E. A review on the photoelectro-Fenton process as efficient electrochemical advanced oxidation for wastewater remediation. Treatment with UV light, sunlight, and coupling with conventional and other photo-assisted advanced technologies. *Chemosphere* **2020**, 126198. [[CrossRef](#)] [[PubMed](#)]
16. Amor, C.; Marchão, L.; Lucas, M.S.; Peres, J.A. Application of advanced oxidation processes for the treatment of recalcitrant agro-industrial wastewater: A review. *Water* **2019**, *11*, 205. [[CrossRef](#)]
17. Vandenberg, L.N.; Luthi, D.; Quinerly, D.A. Plastic bodies in a plastic world: Multi-disciplinary approaches to study endocrine disrupting chemicals. *J. Clean. Prod.* **2017**, *140*, 373–385. [[CrossRef](#)]
18. Plahuta, M.; Tišler, T.; Toman, M.J.; Pintar, A. Toxic and endocrine disrupting effects of wastewater treatment plant influents and effluents on a freshwater isopod *Asellus aquaticus* (Isopoda, Crustacea). *Chemosphere* **2017**, *174*, 342–353. [[CrossRef](#)]

19. Gubitosa, J.; Rizzi, V.; Lopodota, A.; Fini, P.; Laurenzana, A.; Fibbi, G.; Fanelli, F.; Petrella, A.; Laquintana, V.; Denora, N.; et al. One pot environmental friendly synthesis of gold nanoparticles using Punica Granatum Juice: A novel antioxidant agent for future dermatological and cosmetic applications. *J. Colloid Interface Sci.* **2018**, *521*, 50–61. [[CrossRef](#)]
20. Petrella, A.; Spasiano, D.; Rizzi, V.; Cosma, P.; Race, M.; De Vietro, N. Lead ion sorption by perlite and reuse of the exhausted material in the construction field. *Appl. Sci.* **2018**, *8*, 1882. [[CrossRef](#)]
21. Tayo, L.L.; Caparanga, A.R.; Doma, B.T.; Liao, C.H. A Review on the removal of pharmaceutical and personal care products (PPCPs) using advanced oxidation processes. *J. Adv. Oxid. Technol.* **2018**, *21*, 196–214. [[CrossRef](#)]
22. Wang, C.; Kim, J.; Malgras, V.; Na, J.; Lin, J.; You, J.; Zhang, M.; Li, J.; Yamauchi, Y. Metal–organic frameworks and their derived materials: Emerging catalysts for a sulfate radicals-based advanced oxidation process in water purification. *Small* **2019**, *15*, 1900744. [[CrossRef](#)]
23. Oppenlander, T. *Advanced oxidation processes (AOPs): Principles, Reaction Mechanisms, Reactor Concepts*; Wiley VCH: Weinheim, Germany, 2007.
24. Al-Mamun, M.R.; Kader, S.; Islam, M.S.; Khan, M.Z.H. Photocatalytic activity improvement and application of UV-TiO<sub>2</sub> photocatalysis in textile wastewater treatment: A review. *J. Environ. Chem. Eng.* **2019**, *7*, 103248. [[CrossRef](#)]
25. Mascolo, M.C.; Ring, T.A. Recyclable aggregates of mesoporous titania synthesized by thermal treatment of amorphous or peptized precursors. *Materials* **2018**, *11*, 381. [[CrossRef](#)] [[PubMed](#)]
26. Moreira, N.F.; Narciso-da-Rocha, C.; Polo-López, M.I.; Pastrana-Martínez, L.M.; Faria, J.L.; Mania, C.M.; Fernandez-Ibanez, F.; Nunes, O.C.; Silva, A.M. Solar treatment (H<sub>2</sub>O<sub>2</sub>, TiO<sub>2</sub>-P25 and GO-TiO<sub>2</sub> photocatalysis, photo-Fenton) of organic micropollutants, human pathogen indicators, antibiotic resistant bacteria and related genes in urban wastewater. *Water Res.* **2018**, *135*, 195–206. [[CrossRef](#)] [[PubMed](#)]
27. Mascolo, M.C. Synthesis of wide spectrum of mesoporous titania materials by forced co-hydrolysis of Zr–Ti alkoxides. *Micropor. Mesopor. Mater.* **2013**, *181*, 160–165. [[CrossRef](#)]
28. Petrella, A.; Cozzoli, P.D.; Curri, M.L.; Striccoli, M.; Cosma, P.; Agostiano, A. Photoelectrochemical study on photosynthetic pigments-sensitized nanocrystalline ZnO films. *Bioelectrochemistry* **2004**, *63*, 99–102. [[CrossRef](#)] [[PubMed](#)]
29. Camarillo, R.; Rincon, J. Photocatalytic discoloration of dyes: Relation between effect of operating parameters and dye structure. *Chem. Eng. Technol.* **2011**, *34*, 1675–1684. [[CrossRef](#)]
30. Yagub, M.T.; Sen, T.K.; Afroze, S.; Ang, H.M. Dye and its removal from aqueous solution by adsorption: A review. *Adv. Colloid Interface Sci.* **2014**, *209*, 172–184. [[CrossRef](#)]
31. Labidi, A.; Salaberria, A.M.; Fernandes, S.; Labidi, J.; Abderrabba, M. Functional chitosan derivative and chitin as decolorization materials for Methylene Blue and Methyl Orange from aqueous solution. *Materials* **2019**, *12*, 361. [[CrossRef](#)]
32. Tan, I.A.W.; Ahmad, A.L.; Hameed, B.H. Adsorption of basic dye using activated carbon prepared from oil palm shell: Batch and fixed bed studies. *Desalination* **2008**, *225*, 13–28. [[CrossRef](#)]
33. Srinivasan, A.; Viraraghavan, T. Decolorization of dye wastewaters by biosorbents: A review. *J. Environ. Manag.* **2010**, *91*, 1915–1929. [[CrossRef](#)] [[PubMed](#)]
34. Badr, Y.; El-Wahed, M.A.; Mahmoud, M.A. Photocatalytic degradation of methyl red dye by silica nanoparticles. *J. Hazard. Mater.* **2008**, *154*, 245–253. [[CrossRef](#)] [[PubMed](#)]
35. Waghmode, T.R.; Kurade, M.B.; Sapkal, R.T.; Bhosale, C.H.; Jeon, B.H.; Govindwar, S.P. Sequential photocatalysis and biological treatment for the enhanced degradation of the persistent azo dye methyl red. *J. Hazard. Mater.* **2019**, *371*, 115–122. [[CrossRef](#)] [[PubMed](#)]
36. Mittal, A.; Malviya, A.; Kaur, D.; Mittal, J.; Kurup, L. Studies on the adsorption kinetics and isotherms for the removal and recovery of methyl orange from wastewaters using waste materials. *J. Hazard. Mater.* **2007**, *148*, 229–240. [[CrossRef](#)]
37. Lellis, B.; Fávoro-Polonio, C.Z.; Pamphile, J.A.; Polonio, J.C. Effects of textile dyes on health and the environment and bioremediation potential of living organisms. *Biotechnol. Res. Innov.* **2019**, *3*, 275–290. [[CrossRef](#)]
38. Petrella, A.; Boghetich, G.; Petrella, M.; Mastroilli, P.; Petruzzelli, V.; Petruzzelli, D. Photocatalytic degradation of azo dyes. Pilot plant investigation. *Ind. Eng. Chem. Res.* **2014**, *53*, 2566–2571. [[CrossRef](#)]
39. Petrella, A.; Mascolo, G.; Murgolo, S.; Petruzzelli, V.; Ranieri, E.; Spasiano, D.; Petruzzelli, D. Photocatalytic oxidation of organic micro-pollutants: Pilot plant investigation and mechanistic aspects of the degradation reaction. *Chem. Eng. Commun.* **2016**, *203*, 1298–1307. [[CrossRef](#)]
40. Petrella, A.; Spasiano, D.; Cosma, P.; Rizzi, V.; Race, M. Evaluation of the hydraulic and hydrodynamic parameters influencing photo-catalytic degradation of bio-persistent pollutants in a pilot plant. *Chem. Eng. Comm.* **2019**, *206*, 1286–1296. [[CrossRef](#)]
41. Konstantinou, T.; Albanis, A. TiO<sub>2</sub>-assisted photocatalytic degradation of azo dyes in aqueous solution: Kinetic and mechanistic investigations. A review. *Appl. Catal. B Environ.* **2004**, *49*, 1–14. [[CrossRef](#)]
42. Kim, S.H.; Ngo, H.H.; Shon, H.K.; Vigneswaran, S. Adsorption and photocatalysis kinetics of herbicide onto titanium oxide and powdered activated carbon. *Sep. Purif. Technol.* **2008**, *58*, 335–342. [[CrossRef](#)]
43. Tang, W.Z.; An, H. Photocatalytic oxidation of commercial dyes in aqueous solutions. *Chemosphere* **1995**, *31*, 4157–4170. [[CrossRef](#)]
44. Giraldo, A.L.; Penuela, G.A.; Torres-Palma, R.A.; Pino, N.J.; Palominos, R.A.; Mansilla, H.D. Degradation of the antibiotic oxolinic acid by photocatalysis with TiO<sub>2</sub> in suspension. *Water Res.* **2010**, *44*, 5158–5167. [[CrossRef](#)] [[PubMed](#)]
45. Friedmann, D.; Mendice, C.; Bahnemann, D. TiO<sub>2</sub> for water treatment: Parameters affecting the kinetics and mechanisms of photocatalysis. *Appl. Catal. B* **2010**, *99*, 398–406. [[CrossRef](#)]

46. Comparelli, R.; Fanizza, E.; Curri, M.L.; Cozzoli, P.D.; Mascolo, G.; Passino, R.; Agostiano, A. Photocatalytic degradation of azo dyes by organic-capped anatase TiO<sub>2</sub> nanocrystals immobilized onto substrates. *Appl. Catal. B* **2005**, *55*, 81–91. [[CrossRef](#)]
47. Guillard, C.; Lachheb, H.; Houas, A.; Ksibi, M.; Elaloui, E.; Herrmann, J.M. Influence of chemical structure of dyes, of pH and of inorganic salts on their photocatalytic degradation by TiO<sub>2</sub> comparison of the efficiency of powder and supported TiO<sub>2</sub>. *J. Photoch. Photobio. A* **2003**, *158*, 27–36. [[CrossRef](#)]
48. Franco, A.; Neves, M.C.; Ribeiro Carrott, M.M.L.; Mendonca, M.H.; Pereira, M.I.; Monteiro, O.C. Photocatalytic decolorization of methylene blue in the presence of TiO<sub>2</sub>/ZnS nanocomposites. *J. Hazard. Mater.* **2009**, *161*, 545–550. [[CrossRef](#)]